Nanoscale Advances

ROYAL SOCIETY OF CHEMISTRY

PAPER

View Article Online
View Journal | View Issue

Cite this: *Nanoscale Adv.*, 2020, **2**, 356

Controlling wettability, wet strength, and fluid transport selectivity of nanopaper with atomic layer deposited (ALD) sub-nanometer metal oxide coatings†

Yi Li,[ab] Lihua Chen,[a] Jamie P. Wooding,[a] Fengyi Zhang,[c] Ryan P. Lively,[c] Rampi Ramprasad[a] and Mark D. Losego*[ab]

Nanocellulosic films (nanopapers) are of interest for packaging, printing, chemical diagnostics, flexible electronics and separation membranes. These nanopaper products often require chemical modification to enhance functionality. Most chemical modification is achieved *via* wet chemistry methods that can be tedious and energy intensive due to post-processing drying. Here, we discuss the use of atomic layer deposition (ALD), a vapor phase modification technique, to quickly and simply make nanopaper hydrophobic and enhance its wet strength and durability. Specifically, we find that just "a few" ALD cycles (≤10) of either aluminum oxide or titanium oxide is sufficient to significantly increase the durability of cellulose nanofibril (CNF) paper in aqueous media, even under aggressive sonication conditions. Keeping the number of ALD cycles low makes the process more scalable for commodity manufacturing. We investigate whether this increase in wet strength is due to enhanced hydrophobic attractions or stronger hydrogen bonding between CNF fibers. The current evidence suggests that the latter mechanism is likely dominant, with *ab initio* calculations suggesting that newly created M–OH terminations on the cellulose nanofibrils increase hydrogen bond strength between fibers and impede CNF hydration and dispersion. ALD treated nanopapers are also found to preferentially transport hexane over water, suggesting their potential use in oil/water demulsification devices.

Received 2nd July 2019
Accepted 3rd December 2019

DOI: 10.1039/c9na00417c

rsc.li/nanoscale-advances

1. Introduction

Cellulose $(C_6H_{10}O_5)_n$ is a polysaccharide composed of β(1→4) linked D-glucose units. Hydroxyl groups are the prevalent functional group, giving cellulose its hydrophilic nature. Because of its low-cost and sustainable sourcing, cellulosic products are being investigated for a number of technologies including structural composites,[1] flexible electronics,[2,3] microfluidics,[4] and sensors.[5,6] Particularly interesting are composites manufactured from nanocellulosic particles that often show enhanced mechanical performance compared to their microcellulosic fiber analogues.[7,8]

While nanocellulose has a number of attractive properties,[9] modification of the surface chemistry is often desired.[10] Methods for improving nanocellulose dispersion in non-polar matrices for composites, altering surface charge for sorbents, and improving mechanical integrity for membranes are all of interest. To date, surface modification has mostly been accomplished through wet chemical treatments like acetylation,[11] esterification,[12] silanization, silylation,[13] glyoxalization,[14] and polymer grafting.[15] However, wet chemistry modification has drawbacks including tedious solvent exchange processes and complex disposal/separation of waste solvents. These challenges are summarized in ESI Table S1.† Physical treatments like plasma exposures and coatings have also been interrogated, although these can be limited by incomplete conformality.[16] Water resistance is an important property often sought through surface modification.[17] Less attention has been given to the mechanical stability of nanopapers in aqueous environments. Nanopaper-based biosensors, chemical diagnostics, and membranes could all benefit from greater wet strength and aqueous durability.

Recently, several groups have reported on the use of atomic layer deposition (ALD) to modify the surface chemistry of nanocellulosic materials. ALD proceeds *via* a sequential delivery of alternating gas phase precursors and co-reactants to a substrate surface. These gaseous precursors react with the surface chemistry but not with themselves, engendering a self-limiting process

[a]*School of Materials Science and Engineering, Georgia Institute of Technology, Atlanta, Georgia 30332, USA. E-mail: losego@gatech.edu*

[b]*Renewable Bioproducts Institute, Georgia Institute of Technology, Atlanta, Georgia 30332, USA*

[c]*School of Chemical and Biomolecular Engineering, Georgia Institute of Technology, Atlanta, Georgia 30332, USA*

† Electronic supplementary information (ESI) available. See DOI: 10.1039/c9na00417c

that allows for layer-by-layer growth.[18–20] Compared to other thin film deposition techniques, ALD is particularly effective at conformally coating complex geometries with high aspect ratios, including nanostructured materials like nanopaper. Previous studies on the ALD modification of nanocellulose have focused on many ALD cycles (≥100), which results in "thick" metal oxide coatings of >10 nm. While this relatively thick oxide coating effectively protects the nanocellulose from environmental and mechanical degradation, it also reduces mechanical flexibility. Deposition of thick ALD coatings can also often take several hours; reducing this process time would make these treatments more conducive for large-scale manufacturing.

Here, we investigate whether just "a few" ALD cycles (≤10) can improve the mechanical durability of nanopaper. These ALD-treated nanopapers are found to have enhanced durability in aqueous environments, including under aggressive mechanical agitation. The ALD chemistry, layer thickness, and post-annealing thermal treatments all affect this stability. This work reveals evidence suggesting that stronger hydrogen bonding between CNF fibers may be playing a critical role. Density functional theory (DFT) based calculations support this notion, and suggest that newly created M–OH terminations on the cellulose nanofibrils increase hydrogen bond strength between fibers and impede CNF hydration and dispersion. The tunable hydrophobicity of ALD-treated nanopapers also exhibit preferential transportation of oil over water, which make them promising cost-effective oil–water separation devices.

2. Experiment

2.1 Preparation of nanopaper

Cellulose nanofibril (CNF) gel (11.8 wt%) was purchased from the University of Maine Process Development Center. CNFs were dispersed in deionized water *via* overnight sonication. To achieve a uniform nanopaper thickness of ~20 μm, the CNF suspension was adjusted to a solids concentration of 20 g L^{-1}. This CNF suspension was then vacuum filtrated through filter paper (Millipore, 1.2 μm, White RAWP, 90 mm) to create a translucent and compressed CNF freestanding film (nanopaper, Fig. 1(a)). After vacuum filtration, the nanopaper was dried at 50 °C in an oven for 2 h to remove additional water. The final "dried" nanopaper is shown in Fig. 1(b).

These CNF nanopapers were then modified with 1 to 10 ALD cycles of AlO_x or TiO_x. ALD was conducted in a 4″-diameter flow–tube reactor with custom control software.[21] Ultra-high purity nitrogen (Airgas, 99.999%) was used as the process gas. Trimethylaluminum (TMA, Strem, 99%, **DANGER**: Pyrophoric) and titanium tetrachloride ($TiCl_4$, Strem, 97%, **DANGER**: Highly reactive with air, tends to form a corrosive byproduct, HCl) were used as precursors with deionized (DI) water as the co-reactant. Deposition was conducted at 120 °C using the following sequence: 0.5 s TMA (or $TiCl_4$) dose/45 s N_2 purge/0.1 s H_2O dose/45 s N_2 purge. Notation for treatments follow this convention: "*n*cy-ALD AlO_x" or "*n*cy-ALD TiO_x", where "*n*cy" is the number of ALD cycles applied.

2.2 Structural and chemical characterization

Structural and chemical characterization of the nanopaper was carried out with scanning electron microscopy (SEM), Fourier-transform infrared spectroscopy (FTIR), and X-ray photoelectron spectroscopy (XPS). A Phenom ProX SEM was used to study the morphology of cellulose films before and after ALD treatment. FTIR was conducted with a Thermo Scientific Nicolet iS50 FT-IR Spectrometer using an attenuated total reflection (ATR) geometry (diamond crystal). XPS was conducted with a Thermo Scientific K-Alpha system using a monochromatic Al Kα X-ray source (1486.6 eV) with a 60° incident angle and a 90° emission collection geometry. High-resolution scans were taken with a 0.100 eV step size. To minimize cellulose degradation while maintaining reasonable signal to noise, XPS was limited to 3 min high-resolution scans per absorption edge. A detailed discussion of optimizing this X-ray exposure time is included in the ESI, Fig. S1 and S2.† Ellipsometry (Woollam Alpha-SE) was used to estimate the thickness of ALD prepared AlO_x and TiO_x by measuring the film thickness on monitor silicon wafers that were deposited on simultaneously with the nanopapers. A contact angle goniometer (Ramé-Hart 250U-1) was used to measure the static water contact angle (WCA) at 24 °C and 45% relative humidity. A 10 μL volume of DI water was dispersed through a pump and carefully touched to the surface. A CCD camera took pictures of the water droplet after 30 seconds of exposure and the contact angle was assessed with DROPimage software. Five WCA measurements were done on each sample, and an average value was reported in all WCA plots.

2.3 First-principles density functional theory (DFT) calculations

First-principles calculations were used to better understand the chemical mechanisms that may contribute to the enhanced wet

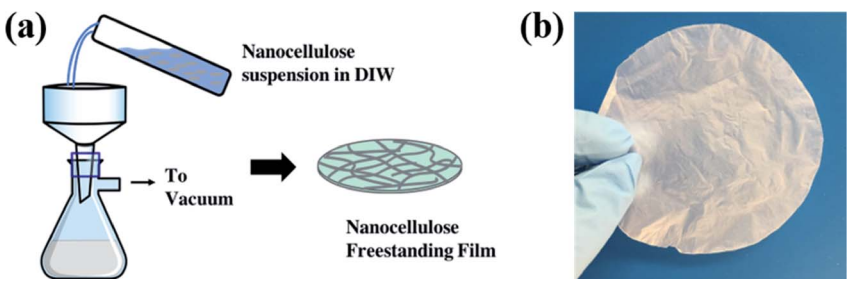

Fig. 1 (a) Schematic of vacuum filtration process and (b) photograph of a CNF nanopaper.

strength of the ALD coated nanopaper. All DFT calculations were performed in the Vienna *Ab Initio* Simulation Package (VASP).[22,23] The Perdew–Burke–Ernzerhof exchange-correlation functional[24] augmented with the vdW-TS functional[25] to properly handle van der Waals interactions was adopted. A plane-wave energy cutoff of 400 eV and a 1 × 1 × 1 Monkhorst–Pack *k*-point mesh were used to relax the structures until atomic forces were smaller than 0.02 eV $Å^{-1}$.

To gain chemical insights, we calculated the dissociation energy (E_{dis}) between two cellulosic "chains" as a function of their chemistry. Four cellulose systems were considered including unmodified, hydrated (H_2O–), $AlO_x(OH)_y$ modified, and $TiO_x(OH)_y$ modified cellulose. The total energy differences between the cellulose systems before and after cleavage were used to approximate E_{dis}. Considering the expensive computational cost of long-chain celluloses and no artificial differences in the E_{dis} trend, 2-layer celluloses, each layer including one repeat unit and terminated by H atoms, were studied. One H_2O molecule was used in the hydrated-cellulose case. In the case of $AlO_x(OH)_y$ modified and $TiO_x(OH)_y$ modified cellulose, two chemical structures were considered: (1) 1 Ti (or Al) atom bonded to each cellulosic layer with 3 OH (or 2 OH) terminating groups, *i.e.*, no chemical bonds connecting the two cellulosic layers, and (2) cellulosic layers connected *via* a M–O–M covalent bond. Five configurations were also computed, including different cellulose orientations, and H_2O, Ti and Al locations for untreated, H_2O–, $Ti(OH)_x$- and $Al(OH)_x$–celluloses to cover the effect of diverse potential structures on the dissociation energy.

2.4 Measurement of nanopaper durability in water

The wet strength of untreated and ALD coated nanopaper was assessed using sonication testing and liquid breakthrough testing. Sonication testing was performed on 1 × 1 cm^2 square coupons (~4 mg). These coupons were sonicated (103 W) in individual vials of 20 mL of deionized water for up to 3 h. At prescribed intervals, aliquots of the aqueous cellulose dispersion were collected. These dispersions were digested in a sulfuric acid (98% H_2SO_4)/anthrone solution (see ESI† for exact procedures). Anthrone is a tricyclic aromatic ketone that is commonly used for colorimetric determination of carbohydrates. The concentrated sulfuric acid (**Caution**: highly corrosive) digests and dehydrates the cellulose into 5-hydroxymethyl furfural. Anthrone conjugates with this furfural, generating a bluish-green color. Optical transmission spectra (AvaSpec-ULS2048L StarLine Versatile Fiber-optic spectrometer) were collected from these aliquots and then compared to an independently prepared calibration standard to quantify the CNF concentration *via* Beer–Lambert's Law (see Fig. S3† for calibration curve).

2.5 Mechanical tensile testing measurements

Uniaxial tensile tests were performed according to a modified-TAPPI T494 method. A MARK-10 ESM303 Mechanical Tester with Series 5 gauge and G1083-2 wedge grips were employed. Specimens were cut into 5 mm × 36 mm strips. Tensile tests were performed with 5 mm min^{-1} rate of crosshead motion. Distance between the grips before the start of test was taken to be specimen gauge length and specimen elongation was taken to be equal to crosshead extension at fracture. For each sample set, at least five specimens were measured.

2.6 Liquid breakthrough testing

Liquid breakthrough experiments were conducted *via* a customized membrane permeation system (*vide infra*, Fig. 8(a)). Nanopaper films were loaded into a stainless steel membrane cell. Prior to testing, the nanopaper and cell were thoroughly dried to remove any residual liquid. Pure water was delivered to the feed side of the membrane cell *via* a 260D syringe pump (Teledyne ISCO) while the purge valve was open in order to release any trapped air. After air purging, the feed pressure is slowly ramped to 10 bar and then increased in 5 bar steps until liquid completely wets and penetrates the films (*i.e.*, liquid is collected from the permeate side; so-called "breakthrough"). At each pressure, the system was equilibrated and observed for 5 min. The reported breakthrough pressures are averages of at least 3 individual measurements on separate nanopapers. Differences in breakthrough pressures reveal differences in hydrophobicity and lipophilicity of the nanopapers. However, unlike WCA measurements, breakthrough testing provides more information about the wettability of the entire fibrous structure, not just the surface.

3. Results

3.1 Basic structural and chemical characterization of untreated and ALD coated nanopaper

The SEM images in Fig. 2 illustrate the typical morphology of our CNF nanopapers. Fig. 2(a) confirms that these nanopapers are ~20 μm thick. Fig. 2(d) and (f) show that ALD coatings of up to 10 cycles of TMA–H_2O (AlO_x) or $TiCl_4$–H_2O (TiO_2) have no significant effects on the micro-scale morphology of the fiber mats. Our best estimate is that at 10 ALD cycles the AlO_x and TiO_x coatings are ≤1.5 nm thick. These thicknesses are based upon spectroscopic ellipsometry measurements made on silicon monitor wafers included in the ALD reactor with the nanopaper and the cumulative ALD literature that has shown these processes to have self-limited growth rates of ~0.11 nm per cycle (TMA–H_2O) and 0.6 nm per cycle ($TiCl_4$–H_2O).[26] Furthermore, both Al and Ti characteristic X-rays were undetectable with EDX spectroscopy, indicating that these coatings are well below the detection limit of this analysis technique (~0.01 wt%).

To confirm the presence of AlO_x and TiO_x coatings, XPS analysis was conducted. Fig. 3(a) shows the survey scans from this XPS analysis. Both Al and Ti are readily detected with XPS. However, even after 10 cycles of AlO_x or TiO_x, the underlying cellulose chemistry can still be detected (C 1s peak and *vide infra*), further confirming that these coatings are less than a few (3 to 5) nanometers thick.

Water contact angle measurements further confirm that the ALD process modifies the nanopaper's surface chemistry. Fig. 3(b) plots the nanopaper's water contact angle as a function

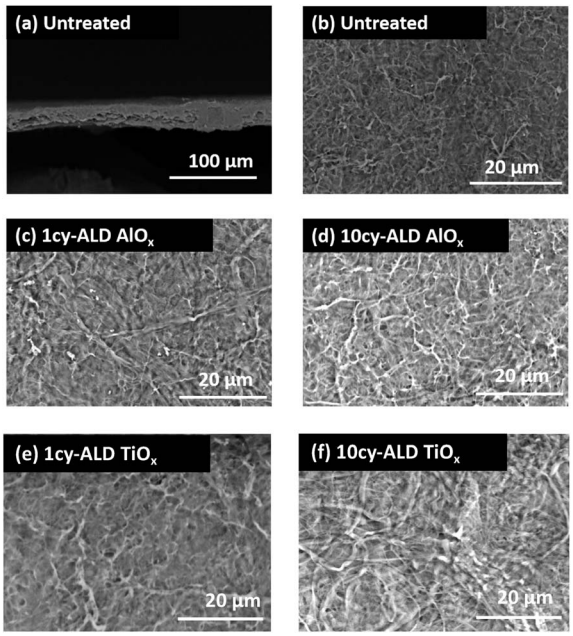

Fig. 2 SEM images of (a) the cross section of an untreated CNF nanopaper and (b–d) plan view images of (b) untreated nanopaper, (c) 1cy-ALD AlO$_x$ treated nanopaper, (d) 10cy-ALD AlO$_x$ treated nanopaper, (e) 1cy-ALD TiO$_x$ treated nanopaper and (f) 10cy-ALD TiO$_x$ treated nanopaper.

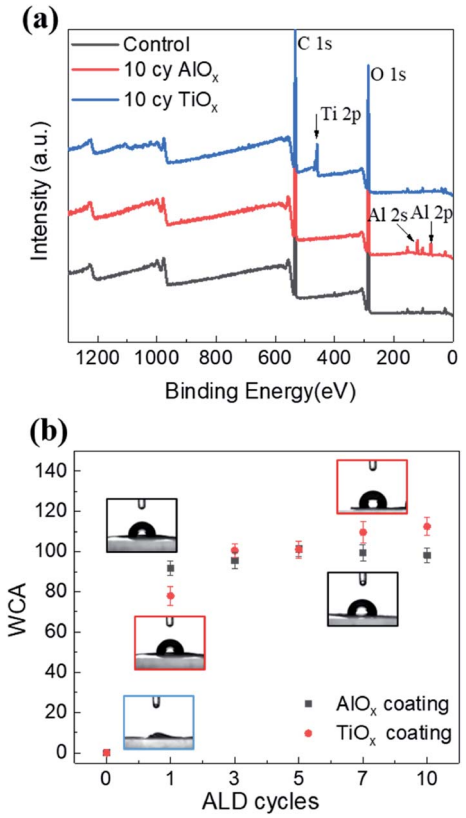

Fig. 3 (a) XPS survey scans of untreated nanopaper, 10cy-ALD AlO$_x$ treated nanopaper and 10cy-ALD TiO$_x$ treate nanopaper; (b) water contact angle for untreated, 1cy-, 3cy-, 5cy- and 10cy-ALD AlO$_x$ and TiO$_x$ treated nanopapers. Error bars show the standard error of five measurements.

of the number of ALD cycles for both the AlO$_x$ and TiO$_x$ chemistries. Like other cellulosic materials, these CNF nanopapers show a significant increase in water contact angle upon 1 ALD cycle of either AlO$_x$ or TiO$_x$.[27–29] While water completely wets untreated nanopaper, water droplets "bead up" (WCA $\geq 80°$) on nanopaper with 1 or more ALD cycles of AlO$_x$ or TiO$_x$. This contact angle can increase to as much as 115°, with more cycles. This hydrophobicity is believed to be the result of hydrocarbons attracted to the ALD deposited metal oxide surface.[29] In XPS we also detect an increase in hydrocarbons on the nanopaper surface, but we cannot differentiate whether their presence is the result of adventitious sources or the chemical degradation of the cellulose *via* exposure to ALD precursor molecules (*vide infra* for discussion). To further confirm that adventitious carbon adsorbs to ALD made oxide thin films, XPS was also conducted on ALD AlO$_x$ and TiO$_x$ thin films deposited on silicon monitor wafers after various "aging" processes, as shown and discussed in Fig. S4 of the ESI.† Regardless of their specific source, we believe these surface hydrocarbons are likely the cause of this increased hydrophobicity. Interestingly, unlike previous reports of metal oxide ALD on cellulosic materials, the hydrophobicity on this nanopaper persists beyond 5 ALD cycles. For example, prior work for ALD treated cotton reported a return to hydrophilicity after about 3 to 5 ALD cycles of AlO$_x$.[28,29]

3.2 Wet strength and durability of ALD coated nanopaper

Fig. 4 is a photographic summary of the increased wet strength of CNF nanopapers modified with ALD. This figure shows photos of untreated and treated nanopapers after 60 min of sonication in water. Immediately evident is that the untreated nanopaper has completely broken apart and dispersed in the water while the ALD coated nanopapers survive with little evidence of degradation.

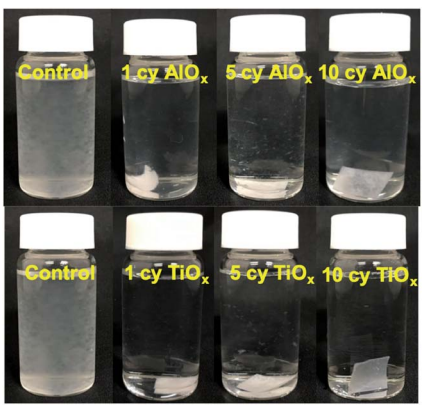

Fig. 4 Photographs of nanopaper in water after sonication for 1 hour. Images show untreated nanopaper (control) and nanopaper coated with (top) 1cy-, 5cy-, and 10cy-ALD AlO$_x$ and (bottom) 1cy-, 5cy-, and 10cy-ALD TiO$_x$.

Fig. 5 provides a quantitative analysis of the concentration of dispersed CNF in water as a function of sonication time for different ALD treatments. (CNF concentration was measured colorimetrically as explained in the Experimental section.) Untreated nanopaper shows rapid degradation within the first 5 minutes and continues to degrade up to 35 min at which point it is fully dispersed. With increasing numbers of ALD cycles, more of the nanopaper is retained for extended sonication times. Durability appears to plateau around 7cy-ALD AlO_x and 5cy-ALD TiO_x. For 10cy-ALD AlO_x, with the AlO_x treatment retaining about 73% of the nanopaper and the TiO_x treatment retaining about 74% of the nanopaper after 2.5 h of sonication. To confirm that the exposure to heat and vacuum during the ALD process did not cause this increased stability, we treated some nanopaper to an ALD process that only dosed water (no metalorganics) for 10 cycles. The control treated nanopapers degraded at the same rate as untreated nanopapers in wet, sonicating conditions (see Fig. S8†). However, we have also found that a post-ALD heat treatment can further increase the wet strength of the nanopaper (Fig. S5†).

Examining Fig. 5 in more detail suggests multiple degradation mechanisms occurring in these nanopapers, some of which are more rapid than others. We suspect these different mechanisms represent different populations of CNFs within the fiber mat. The difference amongst these CNF populations is their extent of bonding to the fiber mat. For example, consider the expanded view of untreated, 1cy-ALD, and 3cy-ALD at short sonication times shown in Fig. 5(c) and (d). For all of these nanopapers, a rapid loss of CNFs is evident within the first 5 min of sonication. In fact, the quantity of this population is the same for both the untreated and 1cy-ALD AlO_x nanopapers (both lose about 44% of their CNFs within the first 5 min). We believe this observation represents the existence of a CNF population that is completely unbound to the nanopaper and is quickly dispersed in the aqueous media. Beyond the first 5 min, the untreated nanopaper shows a CNF loss rate that increases with time until the nanopaper is fully dispersed. In contrast, nanopaper with 3 or more ALD cycles show a degradation rate that generally decreases with time and becomes "stable" at long sonication times. We believe this difference in degradation behavior represents a change in the fiber–fiber attachment mechanism that we discuss in more detail in subsequent sections. Important to note here is that the 1cy-ALD AlO_x treated nanopaper is the only system explored that appears to show all three mechanisms (Fig. 5(d)). It first rapidly loses CNF; it then exhibits a degradation process that increases in rate until about 25 min, at which point its degradation rate begins to slow and plateau similar to the other ALD treated nanopapers. This behavior suggests that the 1cy-ALD AlO_x nanopaper has a population of CNFs that are not yet fully modified by the ALD and become dispersed with a similar rate as the untreated nanopaper.

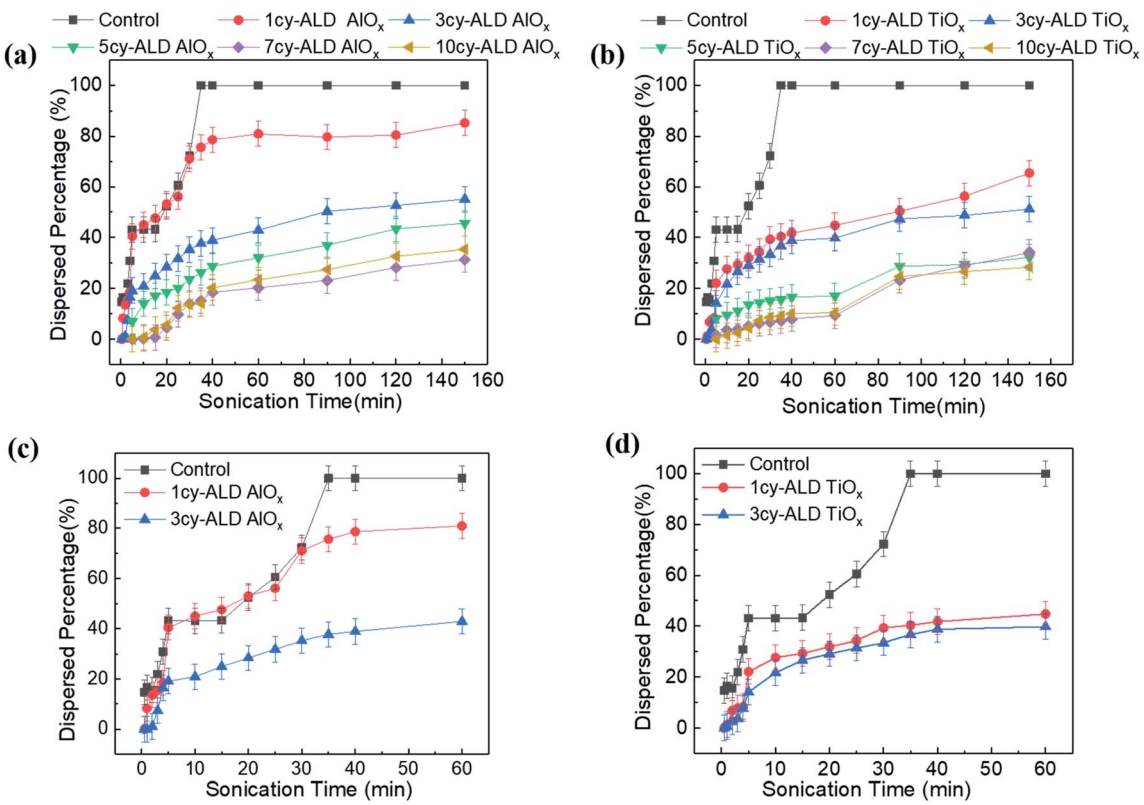

Fig. 5 Concentration of dispersed cellulose as a function of sonication time for nanopaper with (a) *n*cy-ALD AlO_x or (b) *n*cy-ALD TiO_x. Panels (c) and (d) show less sonication time for the untreated, 1cy-ALD and 3cy-ALD nanopapers, providing better clarity to degradation at <5 min of sonication.

3.3 Dry strength of ALD coated nanopapers

Uniaxial tensile measurements were conducted to determine how a few cycles of ALD affect the mechanical strength of nanopaper in the dry state. Fig. 6 plots both the elastic modulus and elongation at break for these nanopapers as a function of the number of ALD cycles. Each data point is the average value for five measurements, and the error bars are the standard deviation of these five measurements. Within this error range, the modulus shows effectively no change from the untreated control nanopaper to ALD modifications of 1, 5, or 10 cycles; variations from control are less than 10% for both chemistries. Elongation at break appears to increase modestly with the number of ALD cycles but is no greater than 20 to 30% than the untreated nanopaper. These results suggest that ALD modification does not enhance dry state strength as much as the wet state strength. This invariability in dry strength is consistent with a previous report for ALD of AlO_x on cellulose fibers.[30]

3.4 Nanopaper membranes for preferential transport of liquids

Because ALD treatments make nanopapers robust in aqueous conditions and tunable in their wettability, we decided to test these materials' effectiveness as membranes for oil/water separations. The interconnected macrovoids within a nanopaper can serve as transport channels for liquids, and the ALD coatings appear to tune the wettability of these channels for liquid selectivity. Fig. 7(a) depicts the liquid breakthrough setup used to test the fluid transport in these membranes. Fig. 7(b) plots the average breakthrough pressures of the nanopaper as a function of ALD cycle number for both water and *n*-hexane. Untreated nanopapers have almost zero contact angle with water thus permeating water with extremely low external pressure ($\sim 0.9 \pm 0.2$ bar). Similarly low pressures are required for *n*-hexane breakthrough, suggesting these untreated membranes would not have good selectivity for oil–water separations. However, applying even just a single ALD cycle of AlO_x or TiO_x to the nanopaper increases the water breakthrough pressure by more than 3× ($\geq$2.7 bar). The water breakthrough pressure continues to rise with additional ALD cycles, while the *n*-hexane breakthrough pressure remains unchanged. At 10cy-ALD AlO_x the breakthrough pressure exceeds 6 bar. This preference in fluid transport suggests the potential of using ALD-treated porous cellulosic media as oil–water demulsification devices. Perhaps most interesting to this study is how with repeated ALD cycle number the breakthrough pressure rises much more

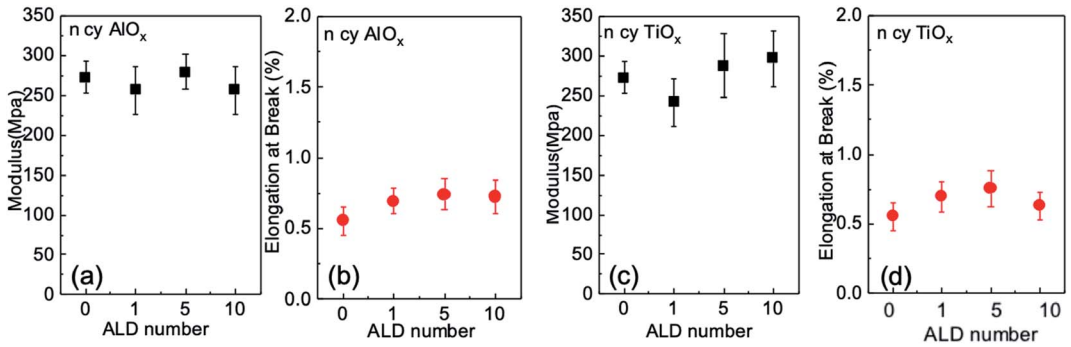

Fig. 6 Uniaxial tensile testing of untreated and AlO_x and TiO_x ALD modified nanopaper: (a and b) modulus and elongation at break as a function of AlO_x ALD cycle number; (c and d) modulus and elongation at break as a function of TiO_x ALD cycle number. All data points are averages of five independent measurements; error bars are the standard deviations of these five measurements.

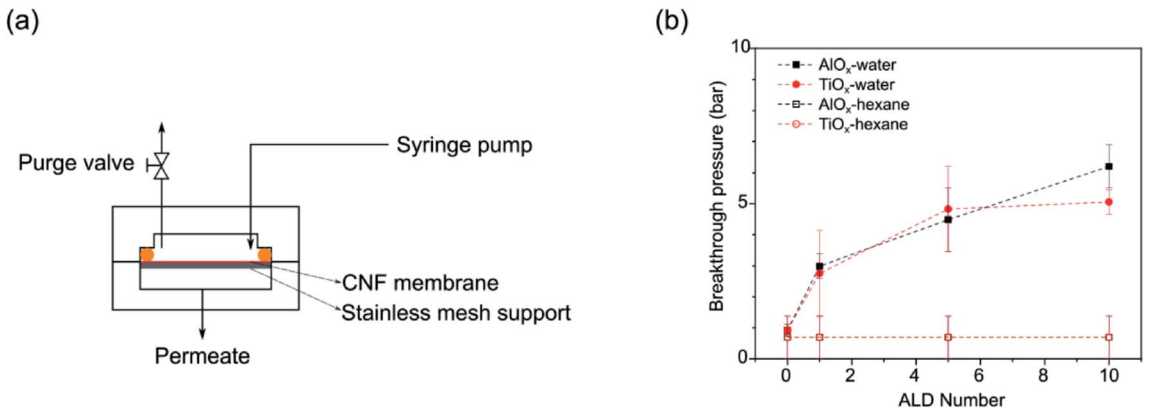

Fig. 7 (a) Schematic of a customized membrane permeation system; (b) aqueous and *n*-hexane breakthrough pressures for untreated, 1cy-, 5cy-, and 10cy-treated AlO_x and TiO_x nanopaper.

sharply than the water contact angle (Fig. 3(b)). Since breakthrough testing is representative of the fluid's ability to wet the entire pore structure, this result potentially suggests that the internal pore structure becomes more hydrophobic with increasing ALD cycle number. Subsequently, we discuss this possibility in more detail and speculate whether stiffer bonding between wetted fibers with increased ALD cycle number may also contribute to this difference in breakthrough pressure.

3.5 Surface chemistry of ALD coated nanopaper

Fig. 8 shows ATR-FTIR spectra for untreated, AlO_x coated, and TiO_x coated nanopaper. The fingerprint regions (Fig. 8(b) and (d)) show no indication of significant changes to the bulk cellulosic structure, but peak intensities do decrease with ALD coating thickness, and more significantly for the TiO_x chemistry. The strong absorptions at 1054–1028 cm^{-1} that corresponds to C–O–C ether group stretches and the small absorption peak at 895 cm^{-1} that corresponds to the cellulosic beta-glycoside linkage stretching remain relatively consistent under all treatment conditions, except after 7 to 10 ALD cycles of TiO_x when the C–O–C absorption bands lose significant intensity. The most obvious change in IR absorption intensity is the broad hydroxyl absorption near 3300 cm^{-1}. The integrated intensity of this absorption reduces by about 40% after a single ALD cycle irrespective of chemistry, suggesting significant consumption of the cellulose's hydroxyl groups. Difficult to differentiate here, though, is the subsequent formation of hydroxyl groups expected to terminate the metal oxide surface after ALD deposition. Consistent with these new hydroxyl group formations is the fact that this hydroxyl absorption intensity remains relatively stable with subsequent ALD cycles.

To further understand the reaction mechanism, XPS spectra of AlO_x coated nanocellulose films are measured and shown in Fig. 9(a)–(f). Fig. 9(a)–(c) are high-resolution, core-level spectra of C 1s, O 1s and Al 2p for *n*cy-ALD AlO_x, while (d) plots the atomic concentrations of carbon binding states for various treatments. The Al 2p peak clearly increases with increasing number of ALD cycles, confirming that more Al is deposited with each ALD cycle. However, the binding energy (B.E.) and peak shape remains constant, implying only one chemical state for Al exists between 1 and 10 AlO_x ALD cycles. Fig. 9(b) indicates that the O 1s binding energy is broadening towards lower binding energies, suggesting that a new type of oxygen bond is forming. We attribute this new binding state to Al–**O**.[31]

Theoretically, the C 1s spectrum of cellulose should exhibit two binding environments for carbon: (1) a C–**C**–O (286.4–286.8 eV) and a O–**C**–O (287.8–288.4 eV). However, the harsh chemical agents used to synthesize nanocellulose inevitably depolymerize and oxidize the cellulose, resulting in the creation of C=O and C–C/C–H groups.[30] Some of the C–C/C–H moieties may also be

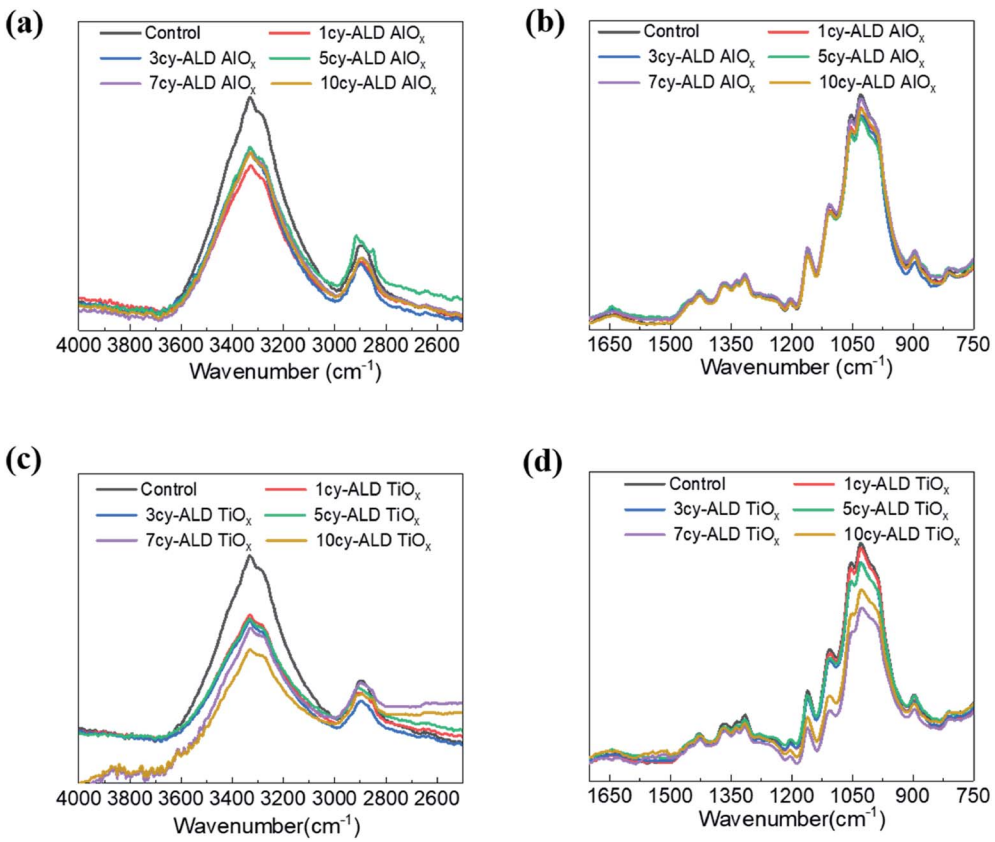

Fig. 8 FTIR spectra of nanopaper with different *n*cy-ALD treatments: (a) 4000–2500 cm^{-1} for *n*cy-ALD AlO_x; (b) 1700–700 cm^{-1} for *n*cy-ALD AlO_x; (c) 4000–2500 cm^{-1} for *n*cy-ALD TiO_x; (d) 1700–700 cm^{-1} for *n*cy-ALD TiO_x.

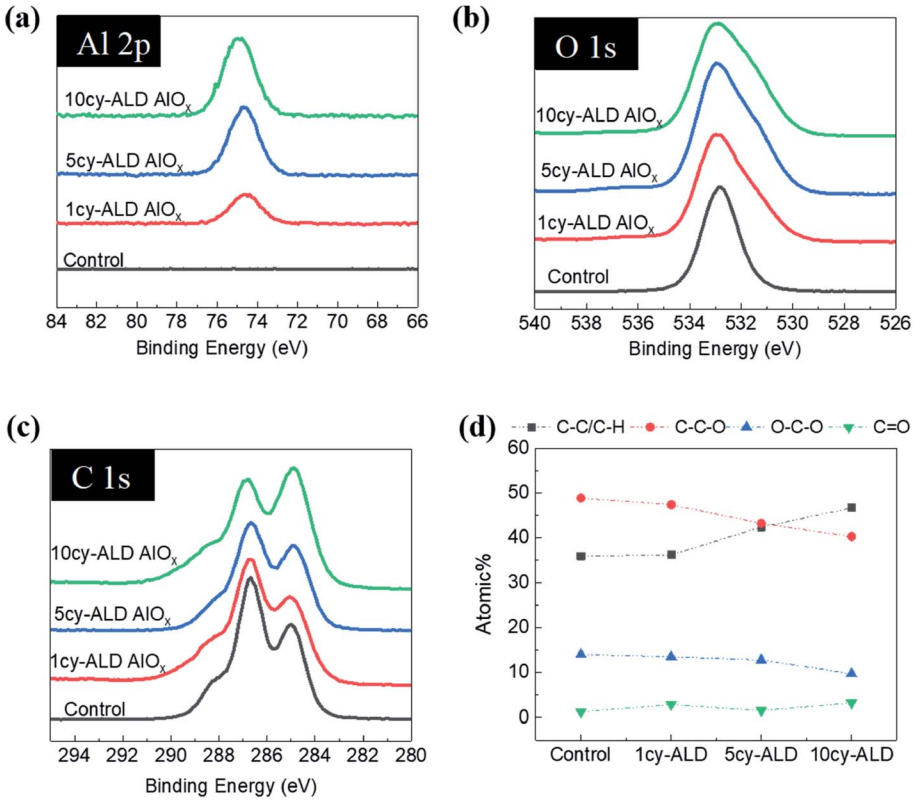

Fig. 9 (a) XPS spectra for *n*cy-ALD AlO_x treated CNF nanopaper. (a) Al 2p spectra; (b) O 1s spectra; (c) C 1s spectra; and (d) atomic percentages of carbon in different bonding environments as a function of nanopaper treatment.

the result of adsorbed adventitious carbon. Fig. 9(d) plots the atomic percentage of **C**–C/**C**–H, C–**C**–O, O–**C**–O and **C**=O in the C 1s core level spectra after deconvolution for *n*cy-ALD AlO_x. With increasing ALD cycle number, the concentration of C–**C**–O groups decreases while the concentration of **C**–C/**C**–H groups increases. One possible explanation for this change in chemistry is continued reactions between TMA and cellulose after all hydroxyl groups are consumed. Fig. 10 depicts the possible reaction sequence. TMA is first believed to react with the cellulose's hydroxyl groups (Fig. 10(a)). Subsequently, TMA may break the β(1–4) glycosidic linkages (Fig. 10(b)), leaving a –O–Al(OH)$_2$ after water exposure. Breakage of this linkage would explain the decrease in C–**C**–O concentration. We speculate that the other half of the broken glycosidic linkage (the one not reacted with TMA) may be methyl terminated, increasing the number of hydrocarbon moieties near the surface and possibly contributing to the nanopaper's hydrophobicity. While a further reaction breaking the C–C–O bonds in the 6-member ring is possible (Fig. 10(c)), we do not see much evidence for the loss of these ring vibrations in the FTIR data (~900 cm^{-1}) a second interpretation of these results is that the increasing ALD thickness is reducing the detectability of the C–**C**–O moieties in the cellulose, and the increase in **C**–C/**C**–H groups is evidence of an increasing quantity of adventitious carbon on the nanopaper's surface. However, regardless of the exact mechanism, we believe this increase in hydrocarbons (**C**–C/**C**–H) on the nanopaper's surface is the source for treated nanopaper's hydrophobicity.

As reported in Fig. 11(a)–(f), similar trends are observed for *n*cy-ALD TiO_x treatments. Here, we note that the C–**C**–O atomic percentage decreases even faster than the TMA chemistry. We suspect that this faster decay is evidence of the HCl byproduct of the $TiCl_4/H_2O$ reaction also degrading the cellulose.[32] The C–**C**–O concentration decreases ~15% after just 1cy-ALD TiO_x and continues to decrease up to 10 cycles.

4. Discussion

Clearly, ALD treatments increase the wet strength of CNF nanopaper. A simple explanation would be that the metal oxide atoms of the ALD coatings encase and/or form linkages between neighboring CNFs to more tightly attach the "connection points" within the CNF network. However, the comparatively modest increase in dry strength after ALD modification observed in Fig. 6 suggests that the more significant increase in wet strength is rather the result of some mechanism triggered by the presence of water. Therefore, we propose two alternate explanations for the observed increase in wet strength of these ALD treated nanopapers: (1) hydrophobic forces[33] increasing the attraction between cellulose nanofibers in aqueous media and/or (2) ALD chemical modification alters inter-fiber hydrogen bonding and CNF hydration. In the following subsections, we discuss the current evidence for and against these proposed mechanisms and discuss their potential contribution to the wet strength.

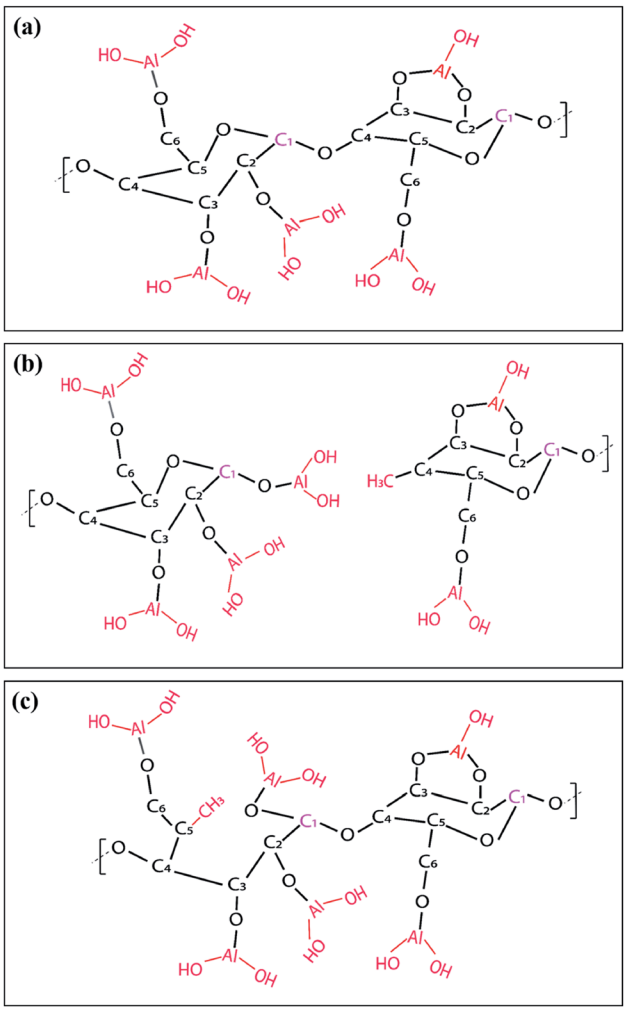

Fig. 10 Schematic of possible reactions that may occur after a single TMA–H_2O ALD cycle: (a) TMA only reacts with cellulose's hydroxyl groups; (b) TMA react with hydroxyl groups and break the β(C_1–O–C_4) glycosidic linkage; (c) TMA reacts with hydroxyls and breaks the carbohydrate ring.

4.1 Hydrophobic attraction amongst CNFs in aqueous media

As shown in Fig. 5(b), CNF nanopaper becomes hydrophobic after ALD coating. This result parallels reports for other cellulosic products including cotton.[19] Presumably, this result implies that the CNFs themselves become more hydrophobic. As a consequence, when immersed in aqueous media, the CNFs should tend to aggregate to reduce the amount of hydrophobic surface area requiring solvation.[33] This thermodynamic driving force towards aggregation could act to increase the wet strength of the CNF nanopaper.

The physical mechanism for the hydrophobic transition of ALD coated cellulose remains unclear. Proposed mechanisms include a physical roughening of the cellulose fiber's surface and an increased attraction of adventitious hydrocarbons to the ALD coated cellulose's surface.[29] Our electron microscopy investigations have not revealed any significant changes in surface morphology, although we cannot completely eliminate possible nano-scale roughening. Chemically, the CNF surface appears to show an increase in **C**–C/**C**–H carbon with ALD treatment. While the exact source of this carbon remains unclear—cellulose depolymerization or adventitious carbon attraction (*vide supra*)—we suspect this surface hydrocarbon is the source of the CNF nanopaper's hydrophobicity.

In an attempt to test whether hydrophobic attraction amongst individual fibers is the source of the nanopaper's enhanced wet strength, we investigated sonication of these ALD treated nanopapers in a variety of non-polar solvents like *n*-hexane and toluene. If the ALD-coated CNF fibers were fully hydrophobic, we would expect the nanopapers to rapidly disperse in these non-polar solvents. However, to this point, we have not found this to be the case. Both the untreated and ALD treated nanopapers have reasonably survived sonication in a variety of non-polar solvents for several hours (see Fig. S8†), suggesting that hydrophobic attractions amongst neighboring CNFs may not be the mechanism for increased wet strength durability.

4.2 Altering CNF hydration and intermolecular bonding

A second explanation for ALD treated nanopaper's increased wet strength is the alteration of chemical bonding between neighboring CNFs. In general, nanocellulose is believed to form from cellulose chains aligning in planar sheets. Neighboring CNFs are interconnected by intermolecular hydrogen bonds and van der Waals forces. In an aqueous environment, water molecules bind to the CNFs, forming water "cages" around the cellulosic chains, disrupting the cellulose–cellulose hydrogen bonds and replacing them with water–cellulose hydrogen bonds. This hydration enables the dispersion of CNFs in water.[34] Since ALD modification of cellulose slows this aqueous dispersion process, another potential explanation is that the cellulose's surface hydroxyl groups are replaced with other bonds that are less susceptible to hydration.

To investigate this possibility, DFT calculations have been performed to calculate the dissociation energy (E_{dis}) between the cellulose layers for varying chemistries. As illustrated in Fig. 12, we examine four cellulosic systems: (1) untreated cellulose, (2) hydrated cellulose (H_2O–), (3) Ti$(OH)_x$ functionalized cellulose (–Ti$(OH)_x$) and (4) Al$(OH)_x$ functionalized cellulose (–Al$(OH)_x$). To better match the XPS results, we have also considered two interfacial structures for each of the metal oxide (MO) chemistries: (A) with M–OH terminations and (B) with M–O–M covalent bond bridges. The black dashed lines in Fig. 11 are the cleavage locations for each system.

The computed E_{dis} values for the four cellulose systems are shown in Fig. 12 and Table 1, in which standard deviations are from five statistical calculations, including different orientations of cellulose, locations of the H_2O, locations of the Ti, and locations of the Al. We note that the dissociation energy increases from H_2O– < untreated < $TiCl_4$– < TMA–celluloses, matching well with the experimental data. Most importantly, the metal oxide terminated surfaces, whether covalently bonded or simply hydroxide terminated, show a dissociation energy increase of at least 2× over either of the unmodified cellulosic

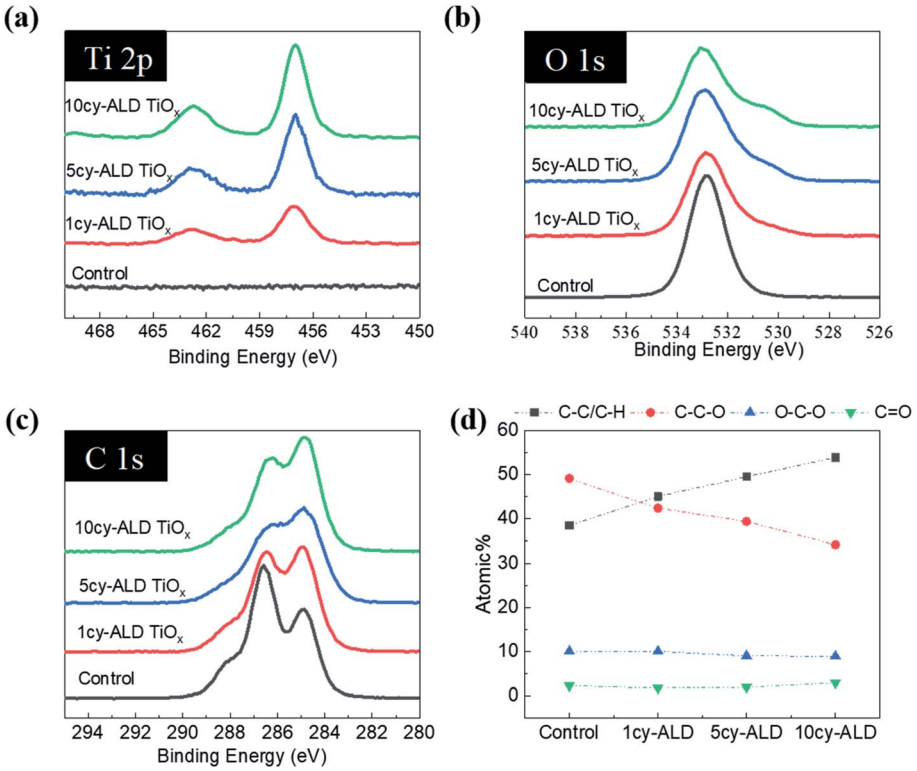

Fig. 11 XPS spectra for *n*cy-ALD TiO_x treated CNF nanopaper. (a) Ti 2p spectra; (b) O 1s spectra; (c) C 1s spectra; and (d) atomic percentages of carbon in different bonding environments as a function of nanopaper treatment.

structures considered. These results suggest that chemical bonds do not need to be formed between two CNFs for greater cohesion between the fibers. Instead, we find that the M–OH terminations (Case A) lead to stronger ion-induced dipole interactions between Ti (or Al) and OH groups compared to the interactions between two hydroxyls on pure cellulose. These calculations suggest that the metal oxide surface chemistry of ALD treated cellulose can strengthen inter-layer interactions in

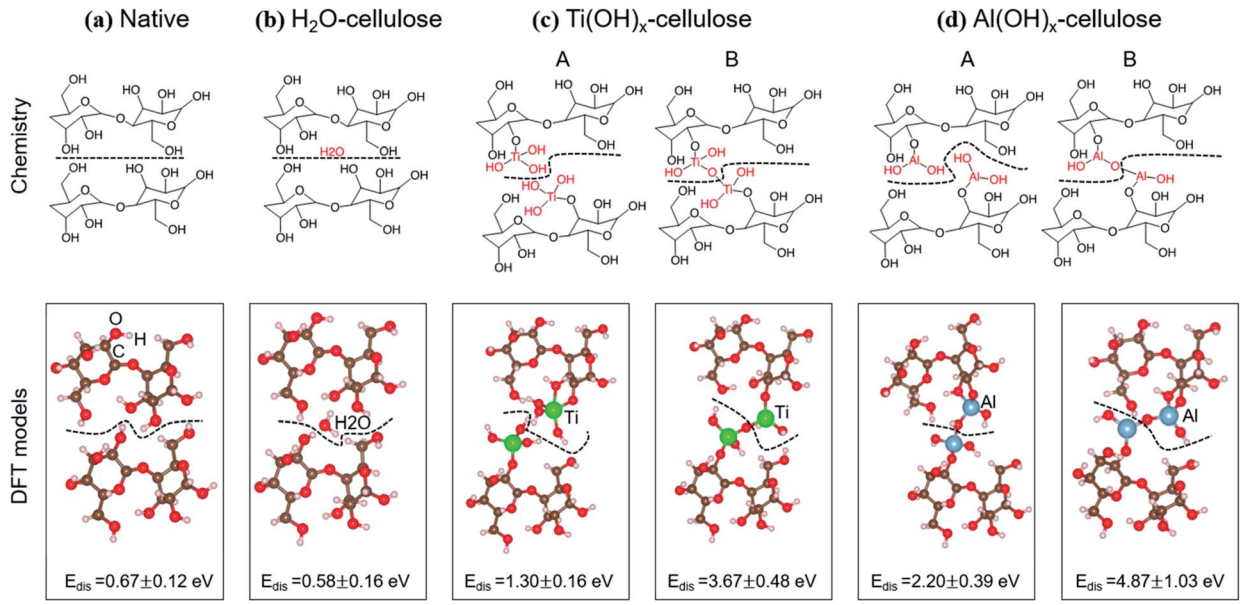

Fig. 12 DFT calculated dissociation energies (E_{dis}) for native, H_2O–, $Ti(OH)_x$ functionalized and $Al(OH)_x$ functionalized cellulose. The standard deviations are from 5 statistical calculations, including different orientations of celluloses, locations of H_2O, Ti and Al for (a)–(d), respectively. Dashed lines denote cleavage locations considered in this study.

Table 1 Summary of DFT calculated dissociation energies (E_{dis}) for native, H_2O–, $Ti(OH)_x$ functionalized and $Al(OH)_x$ functionalized cellulose

System	E_{dis} (eV)
Native	0.67 ± 0.12
H_2O–cellulose	0.58 ± 0.16
$Ti(OH)_x$–cellulose (no –O–Ti–O– bonding)	1.30 ± 0.16
$Ti(OH)_x$–cellulose (with –O–Ti–O– bonding)	3.67 ± 0.39
$Al(OH)_x$–cellulose (no –O–Al–O– bonding)	2.20 ± 0.39
$Al(OH)_x$–cellulose (with –O–Al–O– bonding)	4.87 ± 1.03

aqueous environments relative to pure cellulose, thereby increasing wet strength.

5. Conclusion

This paper reports on the use of a few cycles of metal oxide ALD to modify the surface chemistry, wetting properties, and wet strength of CNF nanopaper. These ALD treatments are found to increase the hydrophobicity of the CNF nanopaper, presumably due to an increase of hydrocarbons at the nanopaper's surface. ALD treated nanopapers with both a TMA–H_2O or $TiCl_4$–H_2O chemistry show increased wet strength under aggressive sonicating conditions. Using DFT calculations, we show that this metal oxide surface modification likely increases the binding energy between CNFs, reducing the probability of water molecules to hydrate the cellulose and drive dispersion. ALD treated nanopapers are also found to be good membranes for preferential transport of *n*-hexane over water, suggesting their potential for use in oil/water demulsification devices.

Conflicts of interest

There are no conflicts to declare.

Acknowledgements

Y. L. was supported through a Renewable Bioproducts Institute Fellowship. JPW was supported by the National Science Foundation Graduate Research Fellowship Program under Grant No. DGE-1650044. This work was performed in part at the Georgia Tech Institute for Electronics and Nanotechnology, a member of the National Nanotechnology Coordinated Infrastructure, which is supported by the National Science Foundation (Grant ECCS-1542174). Any opinions, findings, and conclusions or recommendations expressed in this material are those of the authors and do not necessarily reflect the views of the National Science Foundation.

Reference

1 M. Bolloli, C. Antonelli, Y. Molméret, F. Alloin, C. Iojoiu and J.-Y. Sanchez, Nanocomposite poly(vynilidene fluoride)/nanocrystalline cellulose porous membranes as separators for lithium-ion batteries, *Electrochim. Acta*, 2016, **214**, 38–48.
2 L. Hu, J. W. Choi, Y. Yang, S. Jeong, F. La Mantia, L.-F. Cui and Y. Cui, Highly conductive paper for energy-storage devices, *Proc. Natl. Acad. Sci. U. S. A.*, 2009, **106**(51), 21490–21494.
3 Y. Zhang, L. Zhang, K. Cui, S. Ge, X. Cheng, M. Yan, J. Yu and H. Liu, Flexible Electronics Based on Micro/Nanostructured Paper, *Adv. Mater.*, 2018, **30**(51), 1801588.
4 T. Akyazi, L. Basabe-Desmonts and F. Benito-Lopez, Review on microfluidic paper-based analytical devices towards commercialisation, *Anal. Chim. Acta*, 2018, **1001**, 1–17.
5 S. Alhogail, G. A. R. Y. Suaifan and M. Zourob, Development of Rapid and Low-cost Paper Based Sensing Platform for Bacterial Detection, *Procedia Technology*, 2017, **27**, 146–148.
6 A. M. López-Marzo and A. Merkoçi, Paper-based sensors and assays: a success of the engineering design and the convergence of knowledge areas, *Lab Chip*, 2016, **16**(17), 3150–3176.
7 L. Huang, X. Zhang, M. Xu, J. Chen, Y. Shi, C. Huang, S. Wang, S. An and C. Li, Preparation and mechanical properties of modified nanocellulose/PLA composites from cassava residue, *AIP Adv.*, 2018, **8**(2), 025116.
8 K. P. Y. Shak, Y. L. Pang and S. K. Mah, Nanocellulose: Recent advances and its prospects in environmental remediation, *Beilstein J. Nanotechnol.*, 2018, **9**, 2479–2498.
9 S. Maiti, J. Jayaramudu, K. Das, S. M. Reddy, R. Sadiku, S. S. Ray and D. Liu, Preparation and characterization of nano-cellulose with new shape from different precursor, *Carbohydr. Polym.*, 2013, **98**(1), 562–567.
10 A. Sharma, M. Thakur, M. Bhattacharya, T. Mandal and S. Goswami, Commercial application of cellulose nano-composites – A review, *Biotechnology Reports*, 2019, **21**, e00316.
11 J. Wu, J. Zhang, H. Zhang, J. He, Q. Ren and M. Guo, Homogeneous Acetylation of Cellulose in a New Ionic Liquid, *Biomacromolecules*, 2004, **5**(2), 266–268.
12 L. M. Minsk, J. G. Smith, W. P. van Deusen and J. F. Wright, Photosensitive polymers. I. Cinnamate esters of poly(vinyl alcohol) and cellulose, *J. Appl. Polym. Sci.*, 1959, **2**(6), 302–307.
13 L. Cai, Y. Wang, Y. Wu, C. Xu, M. Zhong, H. Lai and J. Huang, Fabrication of a microfluidic paper-based analytical device by silanization of filter cellulose using a paper mask for glucose assay, *Analyst*, 2014, **139**(18), 4593–4598.
14 F. Quero, M. Nogi, K.-Y. Lee, G. V. Poel, A. Bismarck, A. Mantalaris, H. Yano and S. J. Eichhorn, Cross-Linked Bacterial Cellulose Networks Using Glyoxalization, *ACS Appl. Mater. Interfaces*, 2011, **3**(2), 490–499.
15 D. Roy, M. Semsarilar, J. T. Guthrie and S. Perrier, Cellulose modification by polymer grafting: a review, *Chem. Soc. Rev.*, 2009, **38**(7), 2046–2064.
16 E. B. Gutoff and E. D. Cohen, Water- and solvent-based coating technology, in *Multilayer Flexible Packaging*, ed. Wagner J. R., William Andrew Publishing, Boston, 2010, pp. 163–184, ch. 13.
17 U. M. Garusinghe, V. S. Raghuwanshi, W. Batchelor and G. Garnier, Water Resistant Cellulose – Titanium Dioxide Composites for Photocatalysis, *Sci. Rep.*, 2018, **8**(1), 2306.

18 S. M. George, Atomic Layer Deposition: An Overview, *Chem. Rev.*, 2010, **110**(1), 111–131.
19 G. N. Parsons, S. M. George and M. Knez, Progress and future directions for atomic layer deposition and ALD-based chemistry, *MRS Bull.*, 2011, **36**(11), 865–871.
20 R. L. Puurunen, Surface chemistry of atomic layer deposition: A case study for the trimethylaluminum/water process, *J. Appl. Phys.*, 2005, **97**(12), 121301.
21 B. D. Piercy and M. D. Losego, Tree-based control software for multilevel sequencing in thin film deposition applications, *J. Vac. Sci. Technol., B: Nanotechnol. Microelectron.: Mater., Process., Meas., Phenom.*, 2015, **33**(4), 043201.
22 G. Kresse and J. Furthmüller, Efficient iterative schemes for ab initio total-energy calculations using a plane-wave basis set, *Phys. Rev. B: Condens. Matter Mater. Phys.*, 1996, **54**(16), 11169–11186.
23 G. Kresse and J. Furthmüller, Efficiency of ab-initio total energy calculations for metals and semiconductors using a plane-wave basis set, *Comput. Mater. Sci.*, 1996, **6**(1), 15–50.
24 J. P. Perdew, K. Burke and M. Ernzerhof, Generalized Gradient Approximation Made Simple, *Phys. Rev. Lett.*, 1996, **77**(18), 3865–3868.
25 A. Tkatchenko and M. Scheffler, Accurate Molecular Van Der Waals Interactions from Ground-State Electron Density and Free-Atom Reference Data, *Phys. Rev. Lett.*, 2009, **102**(7), 073005.
26 B. D. Piercy, C. Z. Leng and M. D. Losego, Variation in the density, optical polarizabilities, and crystallinity of TiO_2 thin films deposited via atomic layer deposition from 38 to 150 °C using the titanium tetrachloride-water reaction, *J. Vac. Sci. Technol., A*, 2017, **35**(3), 03E107.
27 J. S. Jur, J. C. Spagnola, K. Lee, B. Gong, Q. Peng and G. N. Parsons, Temperature-Dependent Subsurface Growth during Atomic Layer Deposition on Polypropylene and Cellulose Fibers, *Langmuir*, 2010, **26**(11), 8239–8244.
28 A. E. Short, S. V. Pamidi, Z. E. Bloomberg, Y. Li and M. D. Losego, Atomic layer deposition (ALD) of subnanometer inorganic layers on natural cotton to enhance oil sorption performance in marine environments, *J. Mater. Res.*, 2019, **34**(4), 563–570.
29 K. Lee, J. S. Jur, D. H. Kim and G. N. Parsons, Mechanisms for hydrophilic/hydrophobic wetting transitions on cellulose cotton fibers coated using Al_2O_3 atomic layer deposition, *J. Vac. Sci. Technol., A*, 2012, **30**(1), 01A163.
30 K. E. Gregorczyk, D. F. Pickup, M. G. Sanz, I. A. Irakulis, C. Rogero and M. Knez, Tuning the Tensile Strength of Cellulose through Vapor-Phase Metalation, *Chem. Mater.*, 2015, **27**(1), 181–188.
31 I. Iatsunskyi, M. Kempiński, M. Jancelewicz, K. Załęski, S. Jurga and V. Smyntyna, Structural and XPS characterization of ALD Al_2O_3 coated porous silicon, *Vacuum*, 2015, **113**, 52–58.
32 E. Kontturi, A. Meriluoto, P. A. Penttilä, N. Baccile, J.-M. Malho, A. Potthast, T. Rosenau, J. Ruokolainen, R. Serimaa, J. Laine and H. Sixta, Degradation and Crystallization of Cellulose in Hydrogen Chloride Vapor for High-Yield Isolation of Cellulose Nanocrystals, *Angew. Chem., Int. Ed.*, 2016, **55**(46), 14455–14458.
33 D. Chandler, Interfaces and the driving force of hydrophobic assembly, *Nature*, 2005, **437**(7059), 640–647.
34 T. Budtova and P. Navard, Cellulose in NaOH–water based solvents: a review, *Cellulose*, 2016, **23**(1), 5–55.